CORE
Metadata, citation and similar papers at core.ac.uk
Provided by HKU Scholars Hub
The HKU Scholars Hub The University of Hong Kong 香港大學學術庫

Title	Proteomic approach to study the cytotoxicity of dioscin (saponin)
Author(s)	Wang, Y; Yim, HC; Yang, Z; Chiu, JF; Che, CM; He, QY
Citation	Proteomics, 2006, v. 6 n. 8, p. 2422-2432
Issued Date	2006
URL	http://hdl.handle.net/10722/48497
Rights	Creative Commons: Attribution 3.0 Hong Kong License

Proteomic approach to study the cytotoxicity of dioscin (saponin)

Ying Wang[1], Yim Hing Cheung[2], Zhiqi Yang[1,3], Jen-Fu Chiu[2], Chi-Ming Che[1*], and Qing-Yu He[1*]

[1]Department of Chemistry and Open Laboratory of Chemical Biology, [2]Department of Anatomy, University of Hong Kong, Pokfulam, Hong Kong, China
[3]Shanghai Institute of Organic Chemistry, Shanghai, China

Running title: Proteomics of Dioscin Cytotoxicity

Correspondence to: Dr. Qing-Yu He, Department of Chemistry, University of Hong Kong, Pokfulam, Hong Kong, China. Tel: (852)2299-0787, Fax: (852)2817-1006, E-mail: qyhe@hku.hk

Or: Prof. Chi-Ming Che, Department of Chemistry, University of Hong Kong, Pokfulam, Hong Kong, China. Fax: (852)2857-1586, E-mail: cmche@hku.hk

List of Abbreviations:

DAPI, 4,6-diamidino-2-phenylindole; **IC_{50},** half-maximal inhibitory concentration; **MALDI-TOF MS,** matrix-assisted laser desorption/ionization-time of flight mass spectrometry; $\Delta\Psi_m$, mitochondrial transmembrane potential; **PMF,** peptide mass fingerprinting; **PI,** propidium idodide; **Hsp,** Heat shock protein ; **Rho GDI**, Rho GDP-dissociation inhibitor; **PTPase**, protein-tyrosine phosphatase; **dUTPase,** dUTP diphosphatase; **PPase**, inorganic pyrophosphatase; **hnRNP,** heterogeneous nuclear ribonucleoprotein; **HEI-C,** human enhancer of invasion-cluster.

Abstract

Dioscin, extracted from the root of *Polygonatum Zanlanscianense* pamp, exhibits cytotoxicity towards human myeloblast leukemia HL-60 cells**.** Proteomic analysis revealed that the expression of mitochondrial associated proteins was substantially altered in HL-60 cells corresponding to the dioscin treatment, suggesting that mitochondrion is the major cellular target of dioscin. Mitochondrial functional studies validated that mitochondrial apoptotic pathway was initiated by dioscin treatment. Changes in proteome other than mitochondrial related proteins implicate that other mechanisms are also involved in dioscin-induced apoptosis in HL-60 cells, including the activity impairment in protein synthesis, alterations of phosphatases in cell signaling, and deregulation of oxidative stress and cell proliferation. Current study of protein alterations in dioscin-treated HL-60 cells suggested that dioscin exerts cytotoxicity through multiple apoptosis-inducing pathways.

Keywords: Dioscin / Saponin / Cytotoxicity / HL-60 cells / Mitochondria / Drug mechanism

1. Introduction

Dioscin (Fig. 1), extracted from the root of *Polygonatum Zanlanscianense* Pamp, is one of saponins (plant glucosides). In some traditional Chinese medicine, saponins are major components that have long been used to treat various diseases such as cancers, lung illnesses, palpitation, upset stomach and diabetes [1-3]. Recent biological and pharmaceutical researches showed that diosgenyl saponins exert a large variety of biological functions, with a potential for use in cancer chemoprevention. Dioscin was able to induce cytotoxicity and inhibit the growth of human myeloblast leukemia HL-60 cells [3-6] and Hela cells [7]. The activation of caspase 9 and 3 together with the down-regulation of anti-apoptotic protein Bcl-2, demonstrated that the apoptotic signaling triggered by dioscin was mediated through the intrinsic mitochondria-dependent pathway [3]. Herein we investigated the protein alternations in dioscin-treated HL-60 cells by proteomic approach aiming at globally examining the molecular pathways involved in dioscin-induced cytotoxicity.

Proteomics is a research technique that can identify, characterize and quantitate proteins expressed in cells, tissues or organisms under given conditions such as chemotherapeutic drug treatment [8, 9]. The altered proteins identified by proteomic approach can be further characterized as potential drug targets and the global analysis of the protein alterations can result in valuable information to understand the drug action mechanisms. By comparing the protein profiles of HL-60 cells treated by dioscin to untreated control, we identified differentially expressed proteins by peptide-mass-fingerprinting (PMF). By correlating the proteomic results with other functional studies, the current study provides insights into the action mechanism of dioscin as a potential anticancer drug.

2. Materials and Methods

2.1 Dioscin and other reagents

Dioscin was provided by Shanghai Institute of Organic Chemistry. All other chemicals, except otherwise noted, were purchased from Amersham Biosciences (Uppsala, Sweden). Dioscin was dissolved in Dimethyl Sulphoxide DMSO (Sigma) prior to use.

2.2 Cell lines and culture conditions

HL-60 cells were cultured in RPMI 1640 medium with 2.0 g/L sodium bicarbonate plus 10% fetal bovine serum, 1% L-glutamine, 1% penicillin and streptomycin (100 units/ mL). Those two cell lines were maintained in a humidified incubator with an atmosphere of 95% air and 5% CO_2 at 37˚C. When the cells reached ~80% confluence, they were harvested and plated for either subsequent passages or drug treatments. Cells were treated with 6.6 μg/ml dioscin (7.6 μM) for 24 and 48 hours respectively according to the IC_{50} (Half-maximal inhibitory concentration) measured by Mimaki *et. al.* [4]. After treatment, media was discarded and cells were washed twice with ice cold washing buffer (10 μM Tris-HCl, 250 μM Sucrose, pH 7.0). Cells were then harvested by using a cell scrapper and transferred to a clean 2.0 mL Eppendorf tube, spun down at 3,000 rpm for 5 minutes, and then washed twice with washing buffer, 1 mL each. Cell pellet was lysed by adding 80 μL lysis solution (8 M Urea, 4% CHAPS, 2% IPG buffer, 0.2 mg/mL PMSF). After centrifuged at 14,000 rpm for 10 minutes at 4˚C to clarify the cell lysate, the lysis supernatant was used for 2-DE.

2.3 Morphological changes.

To detect morphological changes in apoptosis process, nuclear staining was performed with 1 μg/ml DAPI, and cells were analyzed by a fluorescence microscope (Olympus IX71 CTS Chinetek Scientific Microscope).

2.4 Flow cytometric analysis of apoptosis.

Dioscin-induced apoptosis was determined with flow cytometry according to the

method previously described [10]. Cells were cultivated for 24 h before either left untreated or treated with 7.6 μM of Dioscin. At the end of each experiment, cells were harvested, resuspended in PBS solution, stained by propidium iodide (PI), and analyzed with a FACStar Plus flow cytometer. For each sample 1×10^6 cells were analyzed, providing a solid statistical basis for the determination of the percentage of apoptotic cells in each treatment using the WinMDI 2.8 software program.

2.5 Two-dimensional electrophoresis (2-DE)

2-DE was performed with Amersham Biosciences (Uppsala, Sweden) IPGphor IEF and Ettan Dalt Six electrophoresis units using the protocol suggested by the manufacturer. Briefly, 80 μg of cell whole protein was mixed up to 250 μL of rehydration solution (8 M Urea, 4% CHAPS, 1 mM PMSF, 20 mM DTT and 0.5% IPG buffer). The rehydration step was carried out with precast 13 cm IPG strips for more than 12 h at low voltage of 30 V. IEF was run following a step-wise voltage increase procedure: 500 V and 1000 V for 1 h each and 5000-8000 V for about 10 h with a total of 64 KVh. After IEF, the strips were subjected to two-step equilibration in equilibration buffers (6 M Urea, 30% Glycerol, 2% SDS and 50 mM Tris-HCl pH 6.8) with 1% DTT (w/v) for the first step, and 2.5% Iodoacetamide (w/v) for the second step. The strips were then transferred onto the second-dimensional SDS-PAGE that was run on 1.5 mm thick 12.5% polyacrylamide gels.

2.6 Silver staining

The gels were fixed with 40% ethanol and 10% acetic acid overnight, and then incubated in a buffer solution containing 30% ethanol, 4.1% sodium acetate and 0.2% sodium thiosulfate for 30 minutes. After washing three times in water for 5 minutes each, the gels were stained in 0.1% silver nitrate solution containing 0.02% formaldehyde for 40 minutes. Development was performed for 15 minutes in a solution consisting of 2.5% sodium

carbonate and 0.01% formaldehyde. EDTA solution (1.46%) was used to stop the development and the stained gels were then washed three times in water for 5 minutes each.

2.7 Image acquisition and analysis

The stained gels were scanned in an Image Scanner (Amersham Biosciences) operated by the software, Lab Scan 3.00, also from Amersham Biosciences. Intensity calibration was carried out using an intensity step wedge prior to gel image capture. Image analysis was carried out using the Image Master 2D Elite software 2003.02 (Amersham Biosciences). Image spots were initially detected, matched and then manually edited. Each spot intensity volume was processed by background subtraction and total spot volume normalization; the resulting spot volume percentage was used for comparison. Only those significantly different spots (over two fold up or down regulate) were selected for analysis by mass spectrometry.

2.8 Tryptic in-gel digestion

Protein spots were excised and transferred into siliconized 1.5 mL Eppendorf tubes. Gel chips were distained in a 1:1 solution of 30 mM potassium ferricyanide and 100 mM sodium thiosulfate and then equilibrated in 50 mM ammonium bicarbonate to pH 8.0. After hydrating with acetonitrile and drying in a Speed Vac, the gels were rehydrated in a minimal volume of trypsin solution (10 μg/mL in 25mM NH_4HCO_3) and incubated at 37˚C overnight. The supernatant was directly applied onto the sample plate with equal amount of matrix. If necessary, the in-gel digests were extracted subsequently with 50% and 80% acetonitrile, and then concentrated and desalted by Zip Tips (Millipore, Bedford, MA, USA) prior to applying on to the sample plate.

2.9 MALDI-TOF MS and protein identification

Tryptic peptide mass spectra were obtained using a Voyage-DE STR MALDI-TOF mass spectrometer (Applied Biosystems, Foster City, CA, USA). The instrument setting was reflector mode with 175 ns delay extraction time, 60-65% grid voltage, and 20 kV

accelerating voltage. Laser shots at 250 per spectrum were used to acquire the spectra with mass range from 600-2500 Da. The trypsin autolytic fragment peaks (906.5049, 1153.5741 and 2163.0570) served as internal standards for mass calibration. Protein identification was performed by searching the NCBInr protein database using MS-Fit (http://prospector.ucsf.edu/). The criteria for searching were set at 50 ppm or better mass accuracy, at least four matching peptide massed and M_r and pI matching estimated values form gels. Post source decay MS/MS measurement and MS-Tag (http://prospector.ucsf.edu/) searching were also performed to confirm the results from MS-Fit. Species search was limited to Homo sapiens.

2.10 Mitochondrial transmembrane potential ($\Delta\Psi_m$)

Changes in mitochondrial transmembrane potential were assayed as described by Huigsloot *et al* [11]. Briefly, after treatment with dioscin for a period of time as indicated, cells were washed twice in HBSS, and incubated with 1 μM Rho-123 (Molecular Probes, Eugene, OR) for 30 min at 37°C. Cells were then washed in HBSS, and resuspended in 1 mL PBS for analysis. Rho-123 (Molecular Probes, Eugene, OR, USA) is taken up selectively by mitochondria [12, 13], and the extent of uptake depends on $\Delta\Psi_m$. Rho-123 fluorescence was measured using a fluorescence-activated cell sorter (Coulter FACS) with excitation and emission wavelengths of 488 and 530 nm. A total of over 10,000 events were analyzed.

2.11 Western blot analysis.

Western blot analysis was performed using primary antibodies against p53 (Santa Cruz), pro-caspase 3 (Santa Cruz), and Bcl-2 (Santa Cruz) respectively at optimal dilution. A nonspecific band from p53 probe was taken as a marker for equal protein loading.

3. Results

Diosin cytotoxicity in HL-60 cells was first verified by morphological observation. Figure 2 shows the morphological changes of HL-60 cells treated with dioscin (7.6 μM) at different time points. Typical apoptotic changes in nuclear were observed in HL-60 cells after dioscin treatment for 16 h, and the number of condensed nucleus increased dramatically after 24 h treatment (Fig. 2A). The numbers of apoptotic cells were quantitated and presented as percentages in Figure 1B.

The effect of dioscin on cell death was further investigated by flow cytometric analysis (Fig. 3). The percentage of the apoptotic cells after dioscin treatment was higher than that in the untreated control cells in a time dependent manner (Fig. 3), with significantly increased apoptosis beginning from 16 h drug treatment, consistent with the results obtained from DAPI staining (Fig. 2). Based on these results, the treatment condition with dioscin 7.6 μM for 24 and 48 h, respectively, was selected for the following proteomic analysis.

Figure 4 shows a pair of representative 2D gel images for whole cell proteins extracted from HL-60 cells with and without dioscin treatments for 24 h. Proteins were well separated in the 2D gels in the ranges of Mr 6 – 200 kD and p*I* 3 – 10. Image analysis revealed that a number of protein spots were significantly altered in terms of volume intensity. Highlighted in circles are the locations where protein alterations were detected. Table 1 lists the proteins' name identified through peptide mass fingerprinting (PMF), together with the spot number, experimental molecular weights and p*I*s, their reported functions and fold differences of alterations corresponding to the dioscin treatments for 24 and 48 hours. Overall, the protein alterations are quite substantial, with fold differences ranging from 2 to 20 folds and consistent changes were observed in both 24 and 48 hour treatments. Table 2 summarizes the parameters resulted from PMF, showing the high mass accuracy and matching scores.

These altered proteins can be classified into several categories according to their known functions. The first group is mitochondrial-related proteins, including the dramatic

increase in the mitochondrial precursors of fumarate hydratase, heat shock protein 60, chaperonin GroEL, ATP synthase alpha and beta chains, and the significant down-regulation of Rho GDP-dissociation inhibitor 1 and 2 (Rho GDIs) and alpha- and beta-tubulins (Table 1 and Fig. 5). The second group of altered proteins involves protein phosphorylation, including the under-expression of protein-tyrosine phosphatase MEG2 (PTPase), dUTP diphosphatase (dUTPase) and inorganic pyrophosphatase (PPase) and the increase of a fragment of ER luminal calcium-binding protein GRP78 (Table 1 and Fig. 6). The third group of proteomic changes contains the down regulation of the nuclear and RNA binding proteins, including RNA-binding protein 28, transformation upregulated nuclear protein and heterogeneous nuclear ribonucleoprotein H (hnRNP H) (Table 1 and Fig. 7). Other protein alterations induced by dioscin include the significant increase of oxidoreductase UCPA, beta tropomyosin and HEI-C and the remarked decrease of glutathione transferase (Table 1 and Fig. 8).

Corresponding to the proteomic changes of mitochondrial proteins, mitochondrial membrane depolarization was measured to test the mitochondrial integrity. In the apoptotic process, the mitochondrial outer membrane becomes permeable, following by releasing cytotoxic proteins from the mitochondrial to the cytosal, and subsequently activated capases [14]. Using Rho-123 as a marker to determine mitochondrial permeabilization, flow cytometric studies showed that the mitochondrial membrane integrity depleted gradually until 24 hour treatment of dioscin (Fig. 9).

Western blot analysis of the mitochondria-associated apoptotic proteins (Fig. 4) revealed that pro-caspase 3 in HL-60 cells disappeared after dioscin treatment for 24 hours, indicating that caspase 3 was activated by the drug treatment. The expression of p53 was detected in 24 and 48 hours treatment of dioscin, and the expression of Bcl-2, the anti-apoptotic protein, was suppressed by dioscin treatment.

4. Discussion

4.1 Dioscin induced apoptosis in HL-60 cells

Natural products are important sources of drugs for the development of novel chemotherapeutics. Diosgenyl saponins are often found as the major components in traditional Chinese medicines, and dioscin is one of the best known diosgenyl saponin [7]. Dioscin has been reported to induce apoptosis in a number of cancer cell lines [3, 7]; however, the detailed mechanisms of dioscin-induced cell death is still unclear. Apoptosis is the process of eliminating unwanted cells in biological systems, and is one of the key mechanisms for chemotherapeutic drugs. There are numbers of typical hallmarks of apoptotic cells, including DNA chromatin fragmentation, DNA laddering, nucleus condensation and PARP-1 cleavage [15, 16]. Figures 2 & 3 showed that dioscin treatment caused marked changes in nuclear morphologies (Fig. 2) and increased the number of cells in the sub-G_1 peak (Fig. 3), suggesting that dioscin exerts cytotoxicity by inducing apoptosis leading to cell death in HL-60 cells.

4.2 Mitochondria is a major target of dioscin cytotoxicity

The substantial alterations of mitochondrial proteins in the dioscin treatment indicate that mitochondrion is a major target of dioscin which impairs the mitochondrial function. The mitochondrial damage induced by dioscin treatment appears the reason for the amount increase of many mitochondrial protein precursors. These proteins may be released from mitochondria before being converted into mature forms due to the mitochondrial dysfunction. This means that the amounts of the functional mitochondrial proteins may be diminished, leading to the decrease of the proteins such as tubulins and Rho GDIs whose proper folding and functioning depend on the mitochondrial proteins. It is well known that mitochondrial HSPs can work cooperatively to bind and fold tubulins and Rho GDIs into the functional molecules [17, 18]. The mitochondrial dysfunction is probably presented as the depletion of mitochondrial potential, as discussed as follows.

Recent studies suggested that mitochondrion plays a central role in the apoptotic process [19]. Once apoptotic signals reached mitochondrion, the outer membrane became permeabilized, releasing apoptotic proteins, for example, cytochrome *c* and apoptosis inducing factor (AIF), into the cytosol, cytochrome *c* thus activates executioner caspases, while AIF translocates into the nucleus to activate nucleases, followed by DNA fragmentation, leading to the morphological and biochemical changes characteristic of apoptotic cell death [20, 21]. Our findings of the depletion of the mitochondrial potential detected 24 hours after treatment of dioscin suggests that dioscin induced apoptosis via mitochondrial initiated death pathways (Fig. 9), followed by the activation of procaspase 3 (Fig. 10).

Biswas *et al* have reported that once the mitochondrion became permeabilized, a number of nuclear gene targets including those involved in Ca^{2+} storage/release (RyR1, calreticulin, calsequestrin), glucose metabolism (hexokinase, pyruvate kinase, Glut4), oncogenesis (TGF-β1, cathepsin L, IGFR1, melanoma antigen) and apoptosis (Bcl-2, Bid, Bad, p53) are upregulated [22]. p53 is a sequence-specific transcription factor that plays a pivotal role in cellular responses to a variety of genotoxic stresses, which result in cell cycle arrest and/or apoptosis [23, 24]. Our data (Fig. 10) showed that p53 expression was significantly up-regulated after mitochondrial membrane potential depletion in response to dioscin treatment. This result indicates that p53 participate in dioscin induced apoptosis downstream of mitochondrion. Bcl-2 family proteins contains anti-apoptotic (Bcl-2 and Bcl-x_L) and pro-apoptotic proteins (Bax and Bad) [25]. Once activated, Bax is inserted into the mitochondrial outer membrane and increases membrane permeability. On the other hand, the anti-apoptotic protein, Bcl-2 inhibits this process, and the balance of Bax and Bcl-2 could decide cell fate of death or survival [26]. The down-regulated Bcl-2 expression as shown in Figure 10 together with the undetectable Bax (data not shown) suggests that the mitochondrial permeabilization is mediated by the regulation of the Bcl-2 family proteins in dioscin treated HL 60 cells.

4.3 Other pathways involved in dioscin cytotoxicity

Proteomic changes other than mitochondrial related proteins implicate that other pathways are also involved in the dioscin cytotoxicity. Dioscin treatment caused the down regulation of several phosphatases (Table 1), suggesting that dioscin may target the cellular signaling pathways, causing the suppression of protein phosphorylation, and leading to the growth inhibition of HL-60 tumor cells. Protein phosphorylation triggers a wide range of cellular signaling pathways that regulate various cellular activities including protein synthesis and cell proliferation. Active protein phosphorylations are thus essential processes for the rapid growth of tumor cells. Dioscin may exert its cytotoxicity by retarding the protein phosphorylation. The increase of the signaling protein fragment (grp78, Table 1) may implicate that the functional phosphoralytion enzyme was degraded during the drug treatment.

The impaired activity of protein synthesis in dioscin treatment can also be derived from the observation of the down regulation of the nuclear and RNA binding proteins (Table 1). These proteins work closely together in protein synthesis process, which is required in cell proliferation and growth. Clearly, dioscin treatment somehow affects the nuclear function and inhibits the protein synthesis process, presenting in the form of the significant suppression of the RNA related proteins. Again, we detected a large increase of a fragment of PAI-1 mRNA-binding protein, suggesting that protein degradation may occur during the drug action. In addition, glutathione transferase is needed to suppress oxidative oxygen species during metabolism and oxidoreductase is an active enzyme in oxidative stress signaling process. The substantial increase of oxidoreductase and the marked decrease of glutathione transferase imply that dioscin treatment actively stimulates the oxidative stress in the leukemia tumor cells, leading to the apoptosis of cell death.

In conclusion, our present experimental results verified that dioscin causes apoptosis of HL-60 cells through nuclear condensation and cell cycle arrest. Proteomic data and mitochondrial functional studies confirmed that mitochondrion is a major target of dioscin.

We further demonstrated that dioscin treatment induces the increase of mitochondrial permeability (mitochondrial potential depletion), leading to the release of mitochondrial functional protein precursors and death initiating proteins. In addition, the dioscin targets also include phosphorylation cellular signaling, RNA-related protein synthesis and oxidative stress processes. These pathways may work complementarily resulting in the severe cytotoxicity of dioscin towards the cancer cells.

Acknowledgements

This work was partially supported by Hong Kong Research Grants Council Grants HKU 7227/02M (to Q.Y.H.), and HKU 7395/03M (to J.F.C.), the Department of Chemistry, and the Areas of Excellence scheme of Hong Kong University Grants Committee.

5. References

[1] (1980) *Flora of China*. Science Publishing Company.

[2] (1986) *Dictionary of Chinese Medicine*. Jiang-Su New Medical College.

[3] Liu, M. J., Wang, Z., Ju, Y., Zhou, J. B. et al, *Biol. Pharm. Bull.* 2004, 27**,** 1059-1065.

[4] Mimaki, Y., Yokosuka, A., Kuroda, M., Sashida, Y., *Biol. Pharm. Bull.* 2001, 24**,** 1286-1289.

[5] Mi, Q., Lantvit, D., Reyes-Lim, E., Chai, H. et al, *J. Nat. Prod.* 2002, 65**,** 842-850.

[6] Wang, Z., Zhou, J., Ju, Y., Zhang, H. et al, *Biol. Pharm. Bull.* 2001, 24**,** 159-162.

[7] Cai, J., Liu, M., Wang, Z., Ju, Y., *Biol. Pharm. Bull.* 2002, 25**,** 193-196.

[8] He, Q. Y. & Chiu, J. F., *J. Cell Biochem.* 2003, 89**,** 868-886.

[9] Wang, Y., Chiu, J.-F., He, Q.-Y., *Current Computer-Aided Drug Design* 2005, 2**,** 563-569.

[10] Lau, A. T., He, Q. Y., Chiu, J. F., *Biochem. J.* 2004, 382**,** 641-650.

[11] Huigsloot, M., Tijdens, I. B., Mulder, G. J., van de, W. B., *J. Biol. Chem.* 2002, 277**,** 35869-35879.

[12] Paquin, J., Danalache, B. A., Jankowski, M., McCann, S. M. et al, *Proc. Natl. Acad. Sci. U. S. A* 2002, 99**,** 9550-9555.

[13] Premkumar, A. & Simantov, R., *J. Neurochem.* 2002, 82**,** 345-352.

[14] Yang, J., Liu, X., Bhalla, K., Kim, C. N. et al, *Science* 1997, 275**,** 1129-1132.

[15] Negri, C., Bernardi, R., Braghetti, A., Ricotti, G. C. et al, *Carcinogenesis* 1993, 14**,** 2559-2564.

[16] Wesierska-Gadek, J., Gueorguieva, M., Wojciechowski, J., Tudzarova-Trajkovska, S., *J. Cell Biochem.* 2004, 93**,** 774-787.

[17] Lund, P. A., Large, A. T., Kapatai, G., *Biochem. Soc. Trans.* 2003, 31**,** 681-685.

[18] Lund, P. A., *Essays Biochem.* 1995, 29:113-23.**,** 113-123.

[19] Rotem, R., Heyfets, A., Fingrut, O., Blickstein, D. et al, *Cancer Res.* 2005, 65**,** 1984-1993.

[20] Affar, E. B., Germain, M., Winstall, E., Vodenicharov, M. et al, *J. Biol. Chem.* 2001, 276**,** 2935-2942.

[21] Araya, R., Uehara, T., Nomura, Y., *FEBS Lett.* 1998, 439**,** 168-172.

[22] Biswas, G., Guha, M., Avadhani, N. G., *Gene* 2005.

[23] el Deiry, W. S., Tokino, T., Velculescu, V. E., Levy, D. B. et al, *Cell* 1993, 75**,** 817-825.

[24] Hartwell, L. H. & Kastan, M. B., *Science* 1994, 266**,** 1821-1828.

[25] Weber, G. F. & Menko, A. S., *J. Biol. Chem.* 2005, 280**,** 22135-22145.

[26] Gross, A., McDonnell, J. M., Korsmeyer, S. J., *Genes Dev.* 1999, 13**,** 1899-1911.

Table 1. Proteins and their alterations after dioscin treatment. Fold differences were calculated based on the image analysis of silver-staining gels.

Spot #	Protein ID (MW/p*I*)	Experimental (MW/p*I*)	Reported function	Fold diff. (24 hr)	Fold diff. (48 hr)
368	Fumarate hydratase, mitochondrial precursor (Fumarase), (54.6 kD/8.8)	54 kD/8.0	Mitochondrial related	+2.1	+2.5
222	Heat shock protein 60, mitochondrial precursor (Hsp60), (61.1 kD/5.7)	60 kD/5.3	Stress-related, chaperone	+2.3	+2.8
1215	Heat shock protein 60, mitochondrial precursor (Hsp60), (61.1 kD/5.7)	60 kD/5.2	Stress-related, chaperone	+6.2	+4.3
297	chaperonin GroEL precursor, mitochondrial matrix protein, (61.1 kD/5.7)	51 kD/5.5	Mitochondrial related	+15.1	+20.0
322	ATP synthase beta chain, mitochondrial precursor (56.6 kD/5.3)	50 kD/5.2	Mitochondrial related	+2.8	+3.5
1255	ATP synthase alpha chain, mitochondrial precursor (59.8 kD/9.2)	60 kD/8.0	Mitochondrial related	+4.0	+4.4
844	Rho GDP-dissociation inhibitor 1 (Rho GDI 1), (23.2 kD/5.0)	23 kD/4.9	Cell differentiation	-3.0	-5.1
868	Rho GDP-dissociation inhibitor 2 (Rho GDI 2), (23.0 kD/5.1)	23 kD/5.0	Cell differentiation	-7.5	-5.5
271	alpha-tubulin, (50.2 kD/4.9)	50 kD/4.9	Cytoskeleton protein	-8.5	-8.3
285	beta-tubulin, (48.9 kD/4.7)	50 kD/4.7	Cytoskeleton protein	-3.4	-3.5
350	Protein-tyrosine phosphatase MEG2 (PTPase-MEG2), (68.0 kD/8.2)	48 kD/6.8	Signaling	-3.9	-10.3
1030	dUTP diphosphatase (dUTPase), (17.7 kD/6.2)	18 kD/5.8	Signaling	-4.1	-9.1
1236	Inorganic pyrophosphatase (PPase), (32.7 kD/5.5)	32 kD/5.5	Signaling	-3.6	-6.3
878	ER lumenal Calcium-binding protein grp78, (72.3 kD/5.1) (N-fragment)	23 kD/5.0	Signaling	+2.1	+2.0
547	Phosphopyruvate hydratase, alpha, (47.2 kD/7.0)	35 kD/5.7	Signaling	-2.5	-3.0
140	RNA-binding protein 28 (85.7 kD/9.3)	85 kD/7.8	Protein synthesis	-4.0	-6.6
207	Transformation upregulated nuclear protein (51 kD/5.2)	55 kD/5.2	Protein synthesis	-3.7	-3.5
312	Heterogeneous nuclear ribonucleoprotein H (hnRNP H), (49.2 kD/5.9)	48 kD/5.9	Protein synthesis	-2.7	-4.8
852	PAI-1 mRNA-binding protein (42.4 kD/8.4) (Fragment)	23 kD/5.0	Protein synthesis	+4.8	+5.5
1081	Oxidoreductase UCPA, (26.7 kD/7.6)	15 kD/5.0	Oxidative	+8.1	+8.5
931	Glutathione transferase, (23.4 kD/5.4)	21 kD/5.3	Oxidative	-2.5	-3.1
919	beta tropomyosin (29.9 kD/4.7)	22 kD/5.1	Cell proliferation	+5.1	+7.9
935	Coiled-coil domain containing protein 5 (Enhancer of invasion-cluster) (HEI-C), (31.9 kD/5.4)	21 kD/5.8	Mitosis	+2.7	+3.0

Table 2. Results of MALDI-TOF mass spectra and database searching for protein identification

Spot #	Protein ID (MW/p*I*)	Acc # (NBCI)	Peptides matched	Sequence coverage (%)	Total mass error (ppm)	MOWSE score
368	Fumarate hydratase, mitochondrial precursor (Fumarase), (54.6 kD/8.8)	1730117	7	16	19	671
222	Heat shock protein 60, mitochondrial precursor (Hsp60), (61.1 kD/5.7)	129379	17	28	24	1037
1215	Heat shock protein 60, mitochondrial precursor (Hsp60), (61.1 kD/5.7)	129379	41	53	18	3.14e+09
297	chaperonin GroEL precursor, mitochondrial matrix protein, (61.1 kD/5.7)	129379	7	23	14	779
322	ATP synthase beta chain, mitochondrial precursor (56.6 kD/5.3)	114549	20	28	15	7.15e+07
1255	ATP synthase alpha chain, mitochondrial precursor (59.8 kD/9.2)	114517	8	18	10	1226
844	Rho GDP-dissociation inhibitor 1 (Rho GDI 1), (23.2 kD/5.0)	1707892	11	57	25	1430
868	Rho GDP-dissociation inhibitor 2 (Rho GDI 2), (23.0 kD/5.1)	1707893	8	37	19	2411
271	alpha-tubulin, (50.2 kD/4.9)	2119266 M	10	22	17	1.44e+05
285	beta-tubulin, (48.9 kD/4.7)	18088719	25	37	15	1.72e+07
350	Protein-tyrosine phosphatase MEG2 (PTPase-MEG2), (68.0 kD/8.2)	1172724	6	17	33	220
1030	dUTP diphosphatase, mitochondrial precursor (dUTPase), (17.7 kD/6.2)	3041664	7	46	20	845
1236	Inorganic pyrophosphatase (PPase), (32.7 kD/5.5)	8247940	5	17	32	161
878	ER lumenal Ca(2+) binding protein grp78, (72.3 kD/5.1) (N-fragment)	87528	10	16	22	3800
547	phosphopyruvate hydratase, alpha, (47.2 kD/7.0)	693933	8	12	19	771
140	RNA-binding protein 28 (85.7 kD/9.3)	55976611	7	11	18	237
207	transformation upregulated nuclear protein (51 kD/5.2)	631470	6	15	29	441
312	Heterogeneous nuclear ribonucleoprotein H (hnRNP H), (49.2 kD/5.9)	1710632	11	23	19	7.17e+04
852	PAI-1 mRNA-binding protein (42.4 kD/8.4) (Fragment)	55665495	5	19	7	283
1081	Oxidoreductase UCPA, (26.7 kD/7.6)	130348	12	41	18	5.08e+05
931	Glutathione transferase, (23.4 kD/5.4)	121746	6	50	34	1.65e+04
919	beta tropomyosin (29.9 kD/4.7)	6573280	6	28	22	465
935	Coiled-coil domain containing protein 5 (Enhancer of invasion-cluster) (HEI-C), (31.9 kD/5.4)	50400607	6	18	31	524

Figure Legends

Figure 1. The chemical structure of dioscin.

Figure 2. Morphological changes of HL-60 cells induced by dioscin.

A. Typical apoptotic morphological changes were detected in dioscin-treated HL-60 cells. The cells were stained with DAPI and visualized by fluorescent microscope (× 320 magnificence).

B. Percentage of apoptotic HL-60 cells under dioscin-treatment.

Figure 3. Flow cytometric analysis indicated that dioscin induced apoptosis in HL-60 cells.

Figure 4. An overview of the master 2D gel images for HL-60 cell extracts. Highlighted in circles are the areas where significant and consistent differences were found in protein expression level.

Figure 5. Detailed alteration patterns of mitochondrial related proteins.

Figure 6. Detailed alteration patterns of the proteins involved in signaling pathways.

Figure 7. Detailed alteration patterns of RNA-binding proteins involved in protein synthesis.

Figure 8. Detailed alterations of proteins involved in oxidative stress and cell proliferation.

Figure 9. Measurement of mitochondrial membrane depolarization in dioscin-treated HL-60 cells by Rho-123 staining.

Figure 10. Western blotting analysis of apoptosis regulating proteins, including p53, pro-caspase 3, and Bcl-2, in dioscin-treated HL-60 cells, using a non-specific band from p53 probe as internal loading control.

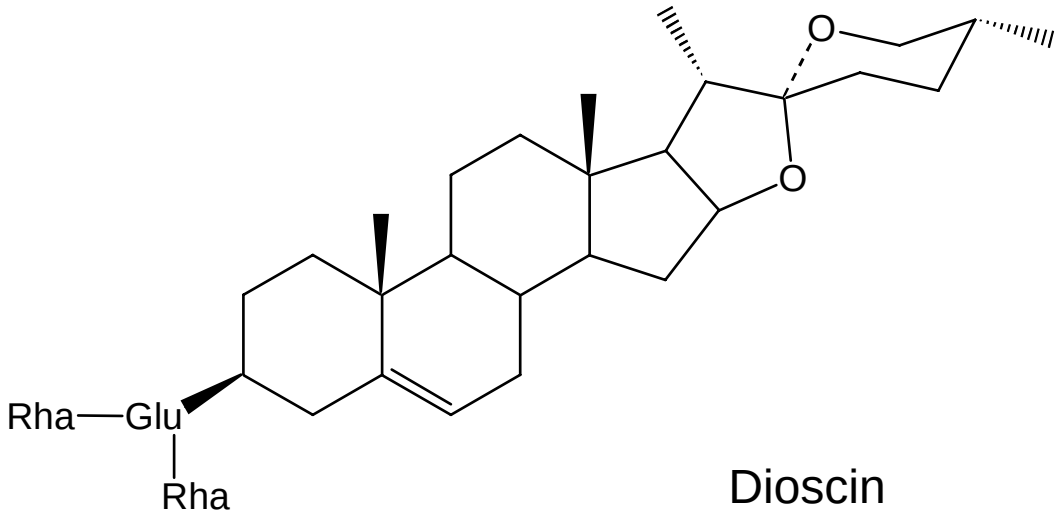

Dioscin

Figure 1

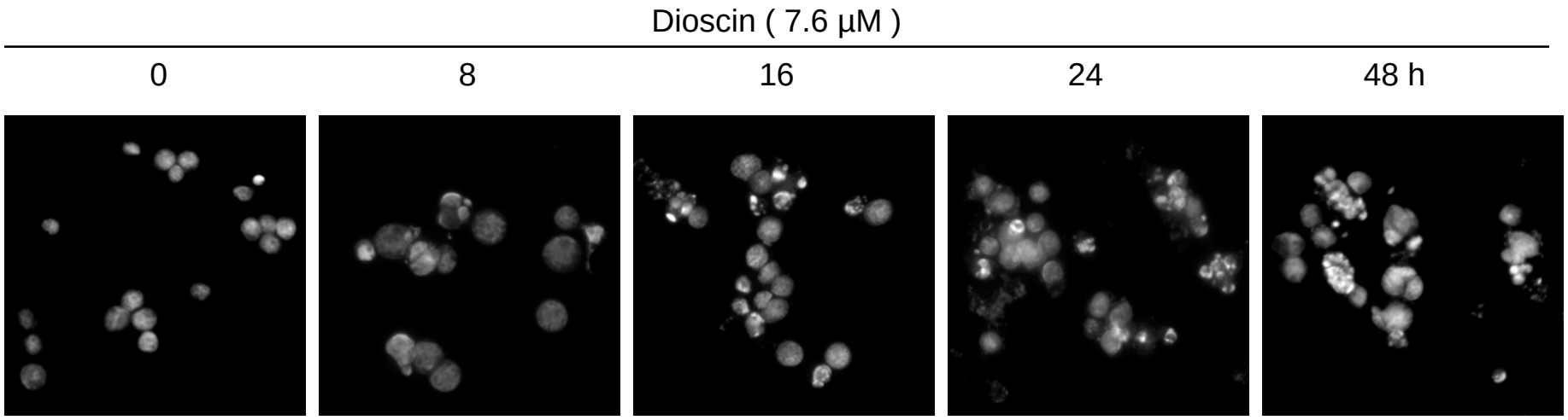

Figure 2A

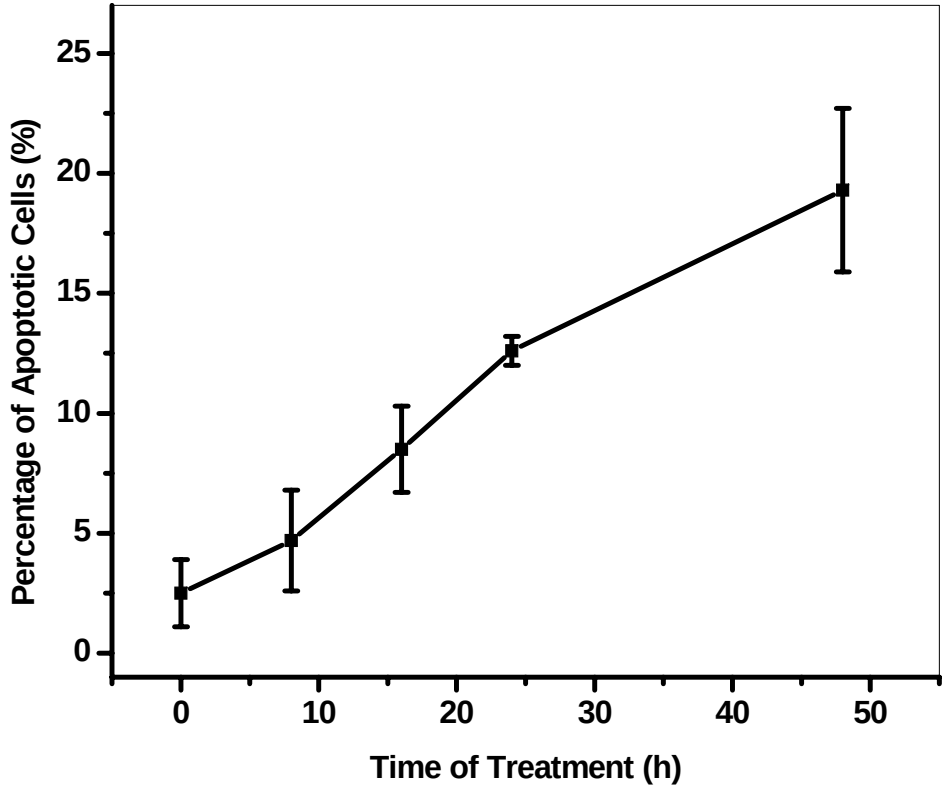
Percentage of Apoptotic Cells (%)
25
20
15
10
5
0
0
10
20
30
40
50
Time of Treatment (h)

Figure 2B

Dioscin (7.6 µM)

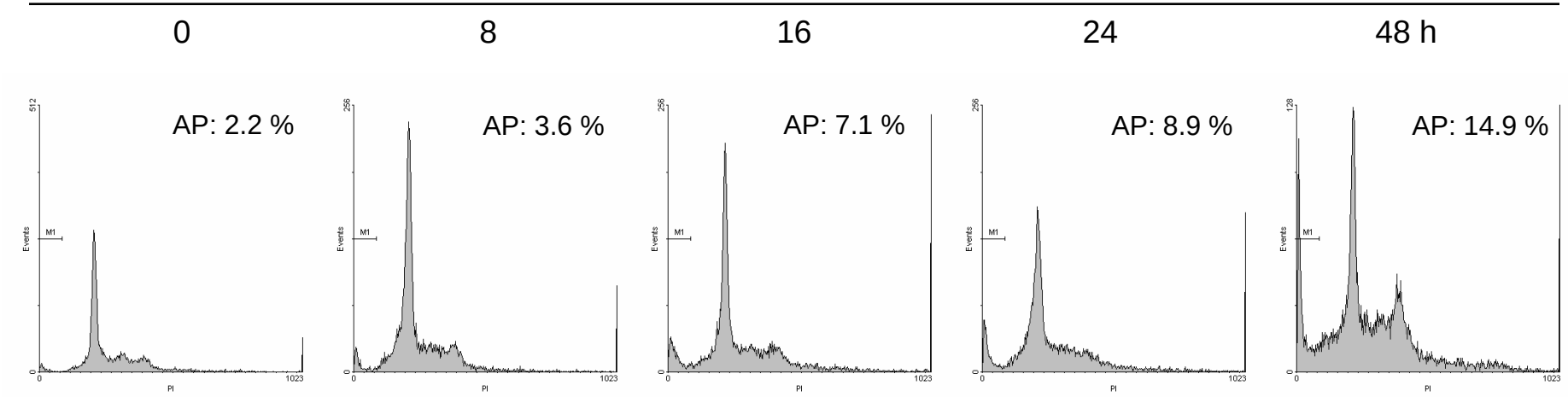

Figure 3

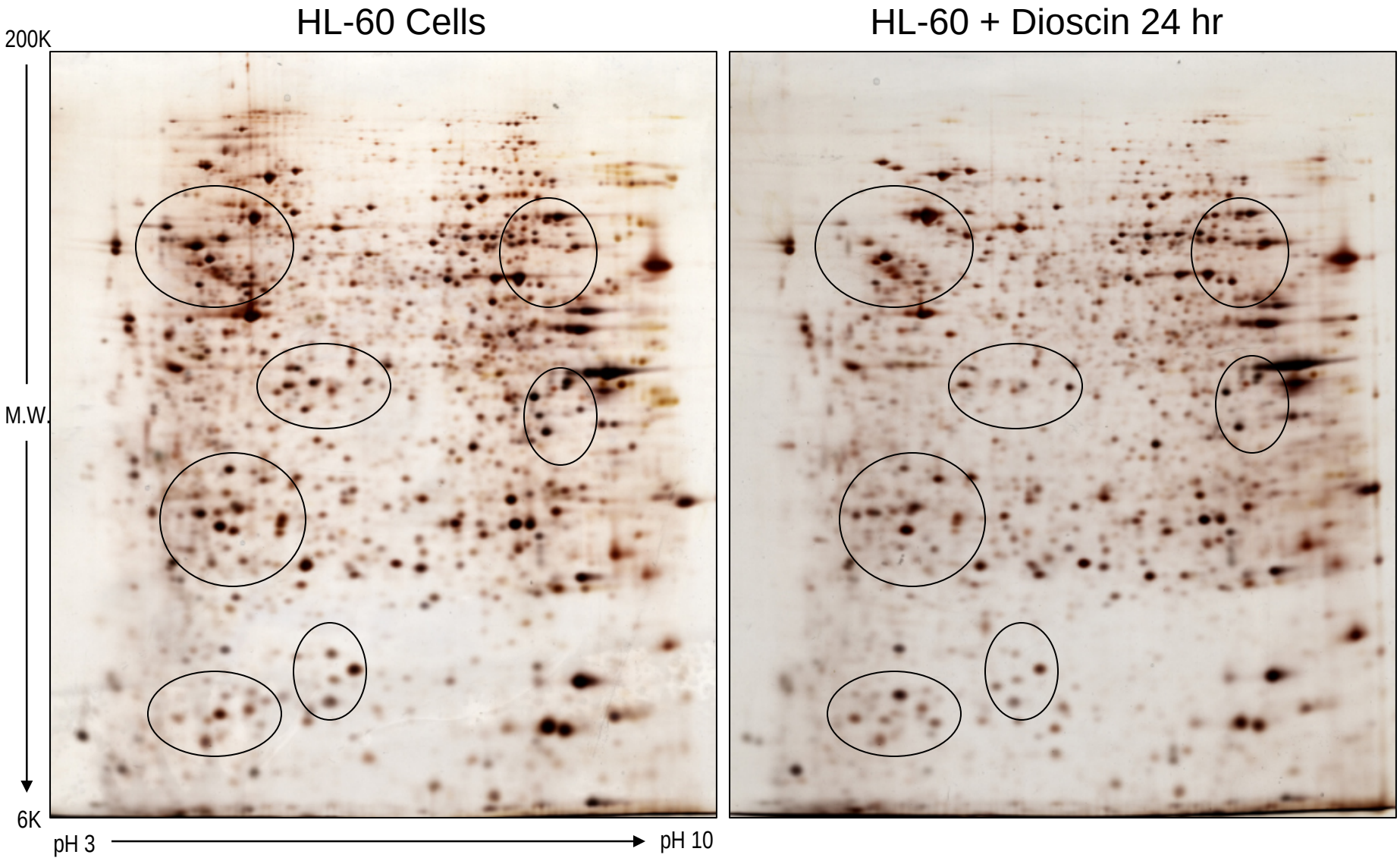

Figure 4

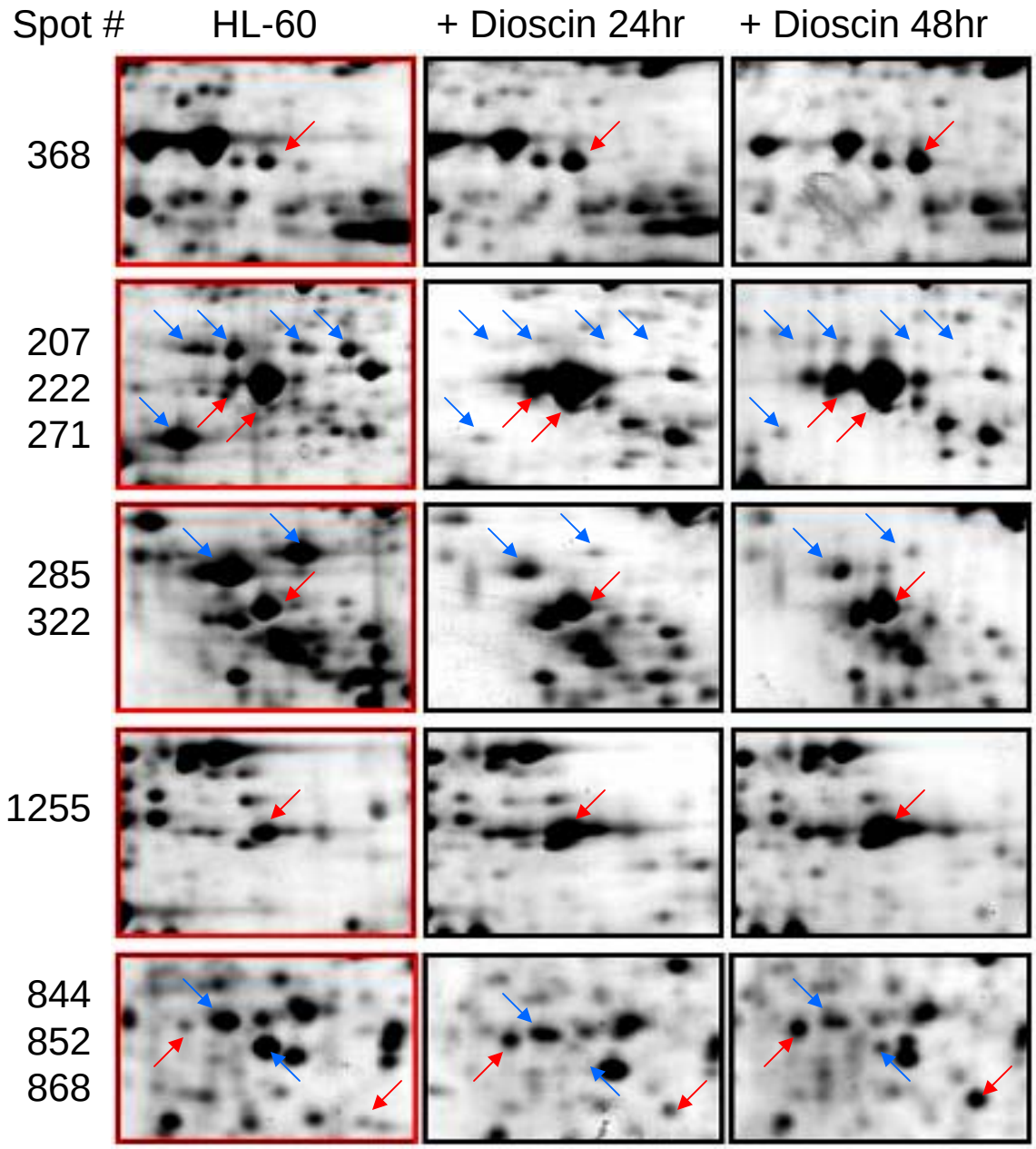
Spot #
HL-60
+ Dioscin 24hr
+ Dioscin 48hr
368
207
222
271
285
322
1255
844
852
868

Figure 5

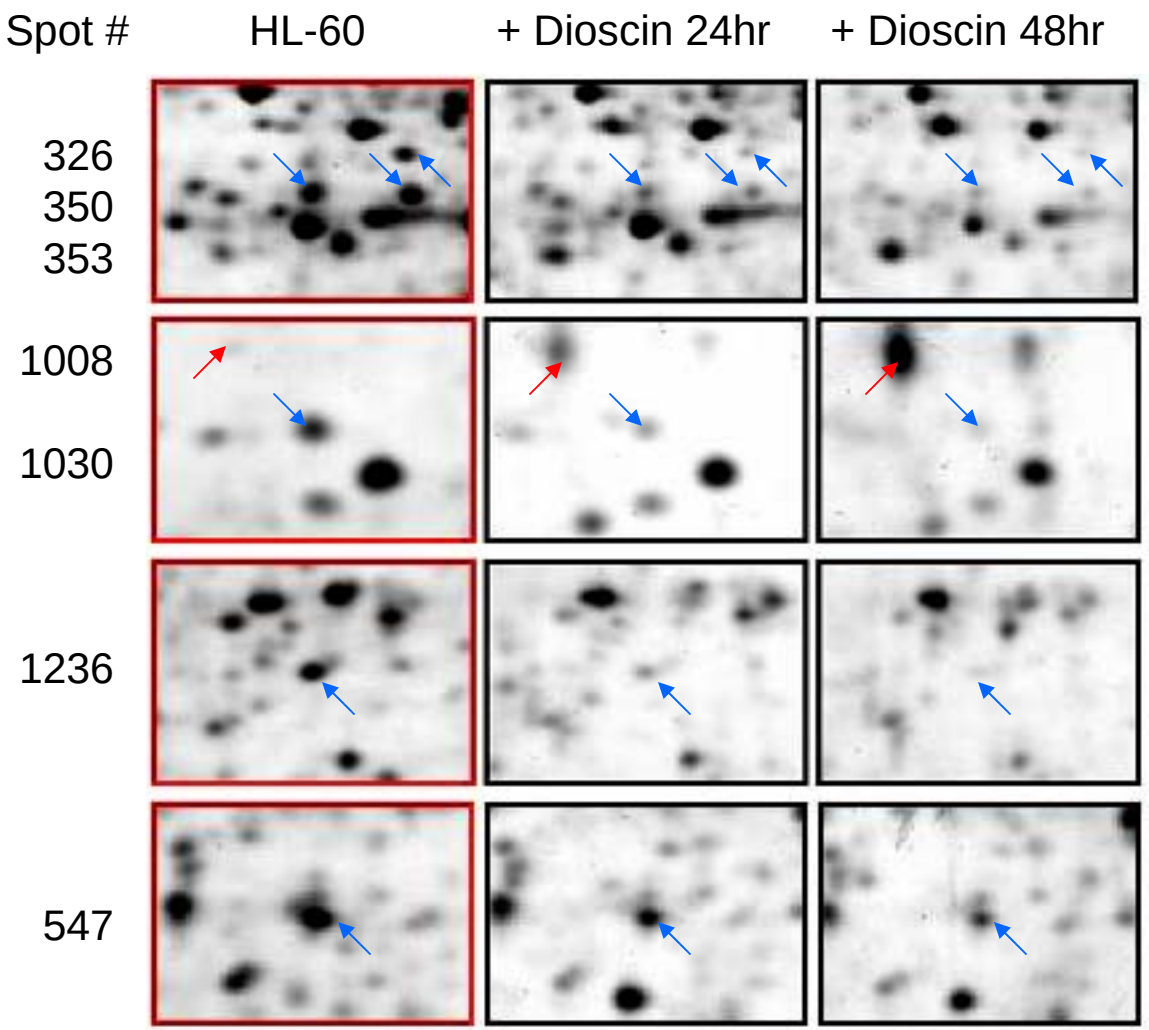
Spot #
HL-60
+ Dioscin 24hr
+ Dioscin 48hr
326
350
353
1008
1030
1236
547

Figure 6

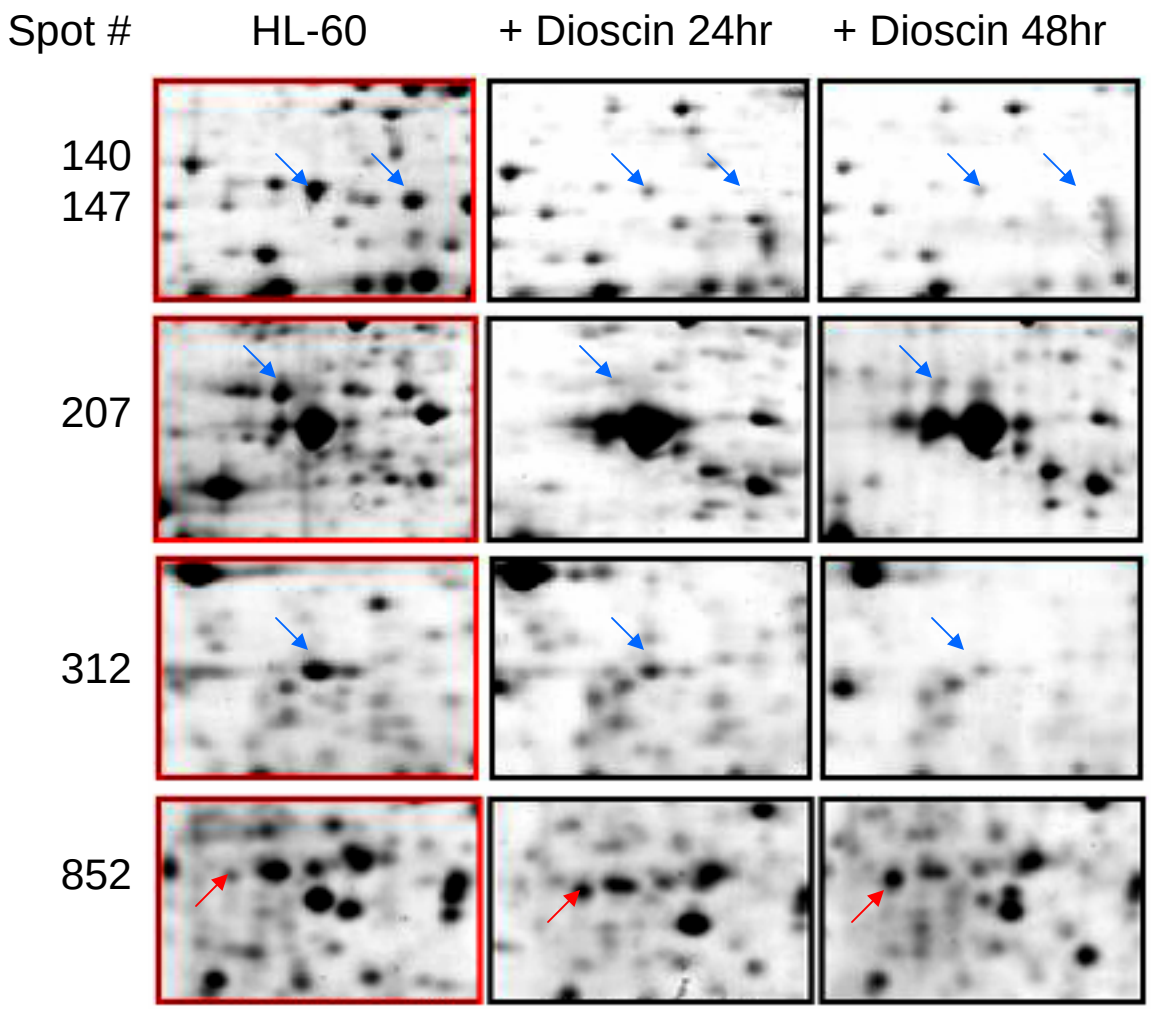

Figure 7

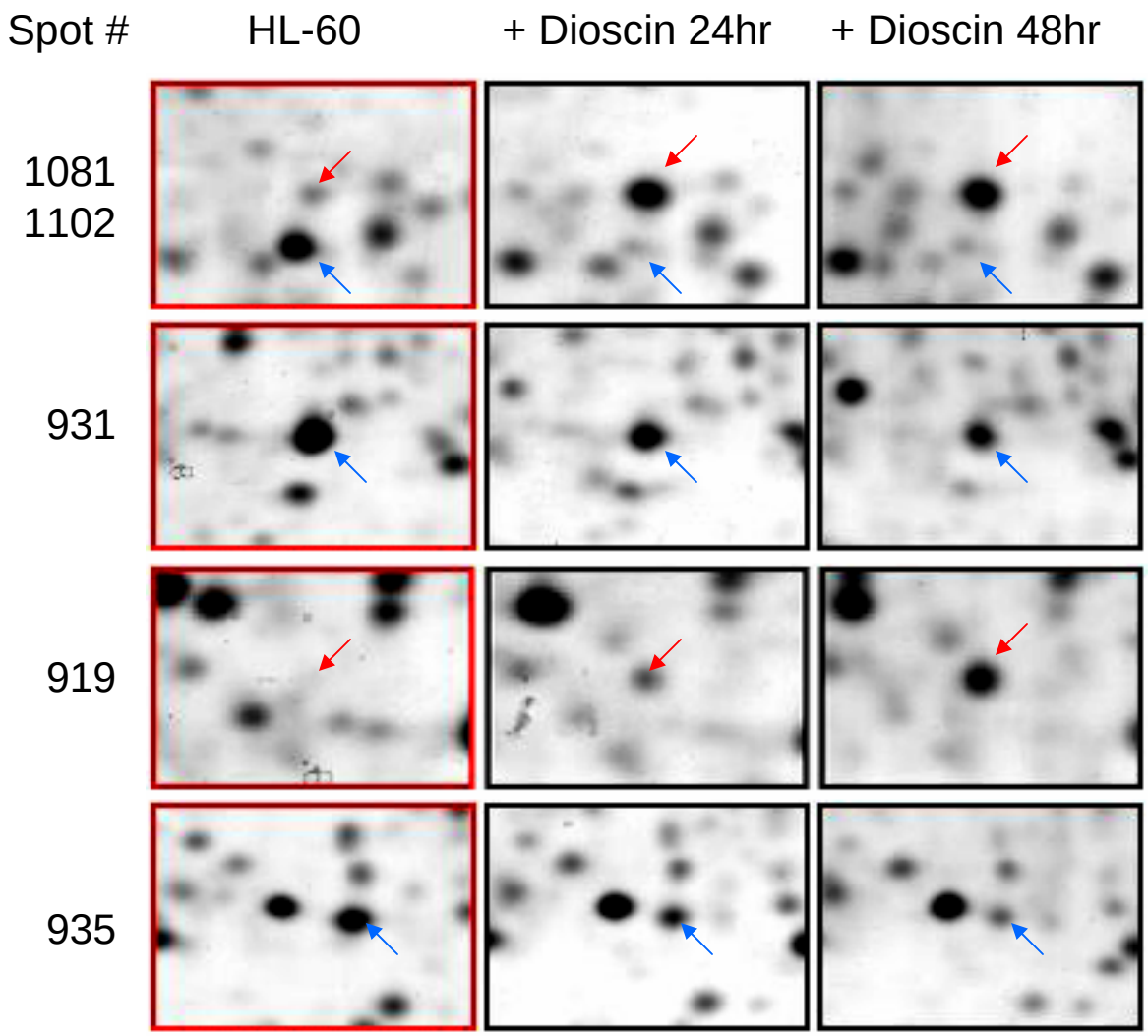

Figure 8

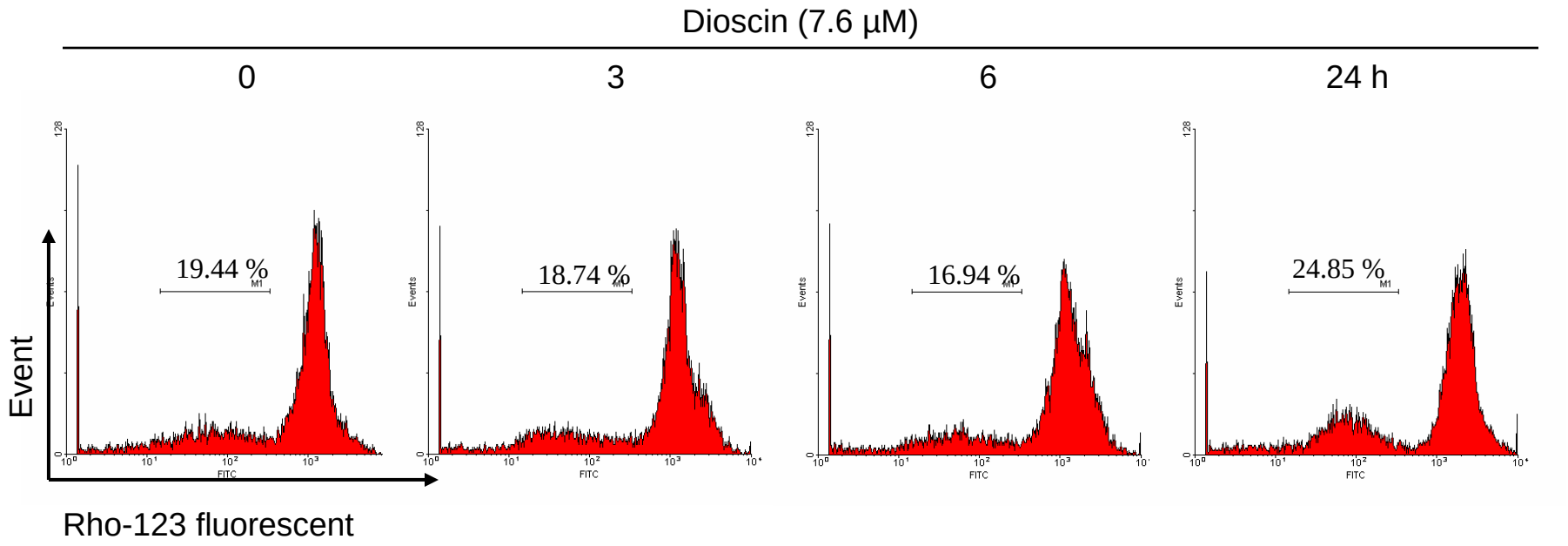
Dioscin (7.6 µM)
0
3
6
24 h
19.44 %
18.74 %
16.94 %
24.85 %
Event
Rho-123 fluorescent

Figure 9

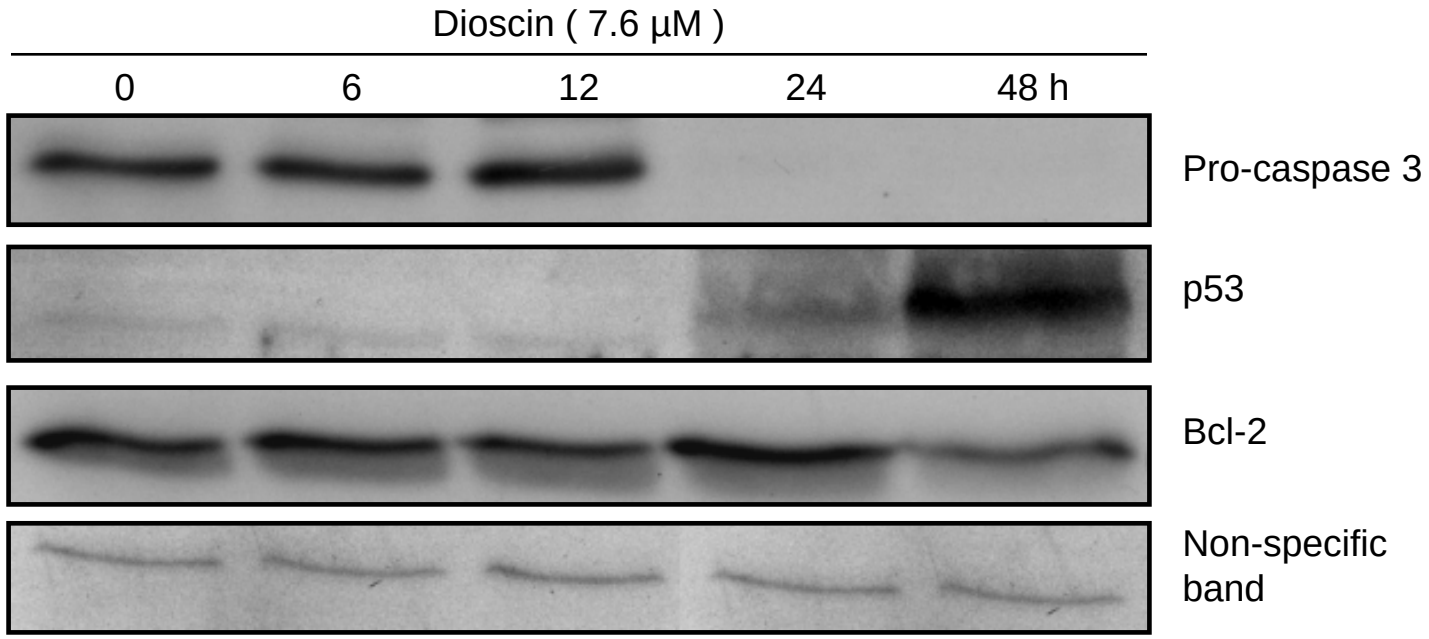
Dioscin (7.6 μM)
0
6
12
24
48 h
Pro-caspase 3
p53
Bcl-2
Non-specific band

Figure 10